Zootaxa 5071 (3): 369–383
https://www.mapress.com/j/zt/

Article

ISSN 1175-5326 (print edition)
ZOOTAXA
ISSN 1175-5334 (online edition)

https://doi.org/10.11646/zootaxa.5071.3.4
http://zoobank.org/urn:lsid:zoobank.org:pub:1AE32395-5C27-4FC8-9006-E899CF866D24

A new phosphatized ophiuroid from the lower Triassic of Nevada and its position in the evolutionary history of the Ophiuroidea (Echinodermata)

BEN THUY[1]*, VIVIENNE MAXWELL[2] & SARA B. PRUSS[2]
[1]*Natural History Museum Luxembourg, Department of Paleontology, 25 rue Münster, 2160 Luxembourg City, Luxembourg.*
[2]*Department of Geosciences, Smith College, Northampton, MA 01063, USA.*
vmaxwell@smith.edu; https://orcid.org/0000-0002-2597-0498
spruss@smith.edu; https://orcid.org/0000-0003-1751-2697
**corresponding author: bthuy@mnhn.lu; https://orcid.org/0000-0001-8231-9565*

Abstract

The Lower Triassic fossil record of brittle stars is relatively rich, yet most records published to date are based on poorly preserved or insufficiently known fossils. This hampers exhaustive morphological analyses, comparison with recent relatives or inclusion of Early Triassic ophiuroid taxa in phylogenetic estimates. Here, we describe a new ophiuroid from the Lower Triassic of Nevada, preserved as phosphatized skeletal parts and assigned to the new taxon *Ophiosuperstes praeparvus* gen. et sp. nov Maxwell, V. & Pruss. S.B. This unusual preservation of the fossils allowed for acid-extraction of an entire suite of dissociated skeletal parts, including lateral arm plates, ventral arm plates, vertebrae and various disk plates, thus unlocking sufficient morphological information to explore the phylogenetic position of the new taxon. Bayesian phylogenetic inference suggests a basalmost position of *O. praeparvus* within the Ophintegrida, sister to all other sampled members of that superorder. The existence of coeval but more derived ophiuroids suggests that *O. praeparvus* probably represents a member of a more ancient stem ophintegrid group persisting into the Early Triassic.

Key words: brittle star, end-Permian mass extinction, phylogeny, fossil

The Late to Early Triassic was a pivotal interval in the evolution of marine communities (e.g. Brayard *et al.* 2017). It witnessed the most extensive mass extinction event so far recorded in Earth history (Sepkoski 1981; Erwin 1993). As a consequence, many of the surviving organismal clades are believed to have undergone a drastic bottleneck followed by a post-extinction radiation (e.g. Twitchett & Oji 2005). However, our understanding of the evolutionary change associated with the end-Permian mass extinction and the subsequent recovery directly depends on the completeness of the fossil record available. In recent years, a number of new fossil discoveries have challenged previous paradigms on faunal change around the Permian-Triassic boundary, including an unexpectedly rapid post-Permian recovery of some marine groups (Brayard *et al.* 2017; Doguzhaeva *et al.* 2018; Botting *et al.* 2019; Brayard *et al.* 2019b; Charbonnier *et al.* 2019; Romano *et al.* 2019; Saucède *et al.* 2019) and the previously unnoticed survival of Paleozoic holdovers (Thuy *et al.* 2017; Thompson *et al.* 2018; Hagdorn 2018).

Ophiuroids, or brittle stars, are one of the five extant echinoderm classes to have survived the end-Permian mass extinction. With respect to their Late to Early Triassic fossil record, they appear to be the best sampled of the five classes, with more than 14 species known from around the boundary interval (Chen & McNamara 2006). A critical re-evaluation of these fossil occurrences, however, debunked most of them as poor, based on insufficiently preserved specimens and/or superficial descriptions, thus precluding their inclusion in phylogenetic analyses (Thuy *et al.* 2019). In fact, for an ophiuroid fossil to be available for phylogenetic studies, it has to be known in sufficient detail to allow comparison with recent relatives (Thuy & Stöhr 2016). The lack of phylogenetically informative ophiuroid fossils from the Late to Early Triassic is particularly unfortunate because the current consensus on the evolution of the class indicates a mid-Permian origin for the crown-group Ophiuroidea followed by a rapid radiation of the major extant clades (O'Hara *et al.*, 2014, 2017; Thuy & Stöhr 2016, 2018).

Here, we describe new ophiuroid fossils from the Lower Triassic of Nevada (Fig. 1). The extraordinary preservation of the fossils, involving replacement of the original skeletal calcite by calcium phosphate (apatite),

Accepted by C. Mah: 15 Oct. 2021; published: 24 Nov. 2021

allowed for acid-extraction of an entire suite of dissociated skeletal plates from limestone, unlocking sufficient morphological information to allow inclusion of the new ophiuroid in a phylogenetic analysis.

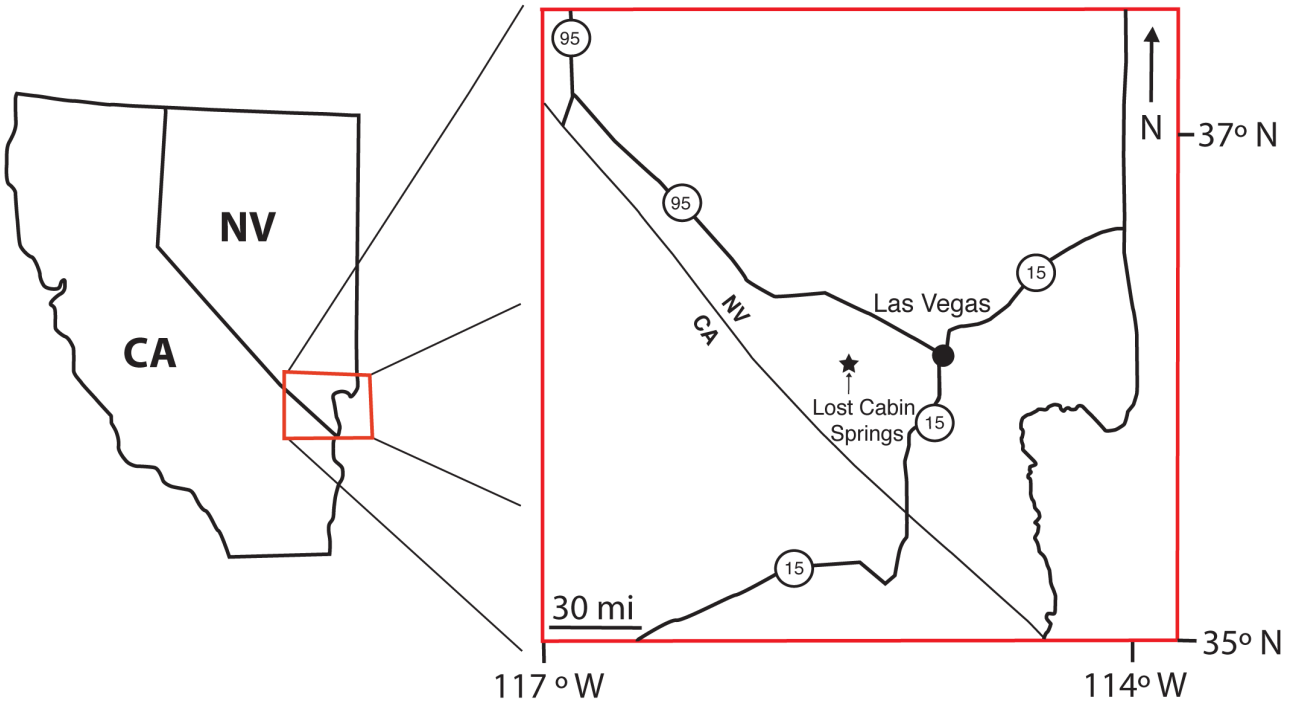

FIGURE 1: Locality map of the Virgin Limestone Member at the Lost Cabin Springs Locality, Southern Nevada, Western United States (36°4′57.18′N, 115°39′12.05′W is near the base of the section). (modified from Maxwell, 2020).

Geological Context

During the Early Triassic, the western United States was situated at a tropical paleolatitude (Reif & Slatt, 1979). The Lower Triassic Moenkopi Formation extends throughout the Colorado Plateau and into southern Nevada and its depositional environment gradually shifts from continental fluvial sedimentation in Arizona to more intertidal and shallow marine environments in Utah and Nevada (Reif & Slatt, 1979). The Moenkopi Formation in southern Nevada was deposited in a shallow water setting on the eastern margin of the Panthalassa sea (Marzolf, 1993) (Fig. 2). The non-marine Timpoweap Member or the Lower Red Member is overlain by the Virgin Limestone Member, which is in turn overlain by the evaporitic Shnabkaib Member (Reif & Slatt, 1979). The Virgin Limestone Member of the Moenkopi Formation is a mixed carbonate-siliciclastic succession (Poborski, 1953). At the Lost Cabin Springs locality, it is constrained to the Spathian Stage (late Early Triassic) (Poborski, 1953) and was deposited in a storm-dominated subtidal paleoenvironment (Schubert & Bottjer, 1995; Pruss *et al.*, 2005). There is an abundance of unusual facies present in the Virgin Limestone Member, including microbialite facies, such as large microbial reef mounds that span the length of the Lost Cabin Springs outcrop area (Pruss & Bottjer, 2004), wrinkle structures (Pruss *et al.*, 2004), and flat-pebble conglomerate facies (Pruss *et al.*, 2005). Of eight fossiliferous samples, ophiuroids were only present in Bed LC–18–34 (Maxwell *et al.*, 2020). Approximately 115 meters from the base, this bed is a thin 3.5 m-thick fossiliferous packstone with isolated crinoidal ossicles overlying a small microbial build-up.

Material and Methods

In 2018 and 2019, samples of fossiliferous packstone were collected and dissolved in 200 – 400 ml of 10% glacial acetic acid solution buffered with ammonium acetate, and only one sample (LC–18–34) produced abundant ophiuroid fragments. The insoluble residues were sieved into the following size fractions: >400 µm, >250 µm and >177 µm, and the ophiuroid elements were common components of the >400 µm and >250 µm fractions. The sieved samples were examined under the Nikon SMZ645 stereoscopic microscope, and an Olympus BHS BH-2 light microscope

was used to image these fossils. The best preserved ophiuroid elements (n=71) were coated with gold and palladium by a Hummer V Sputter coater and imaged with the FEI Quanta 450 Scanning Electron Microscope (SEM) at Smith College and with the Jeol Neoscope JMC-5000 SEM at the Natural History Museum Luxembourg. The elemental composition of the fossils was analyzed using EDS (Energy Dispersive Spectroscopy) Team software at Smith College.

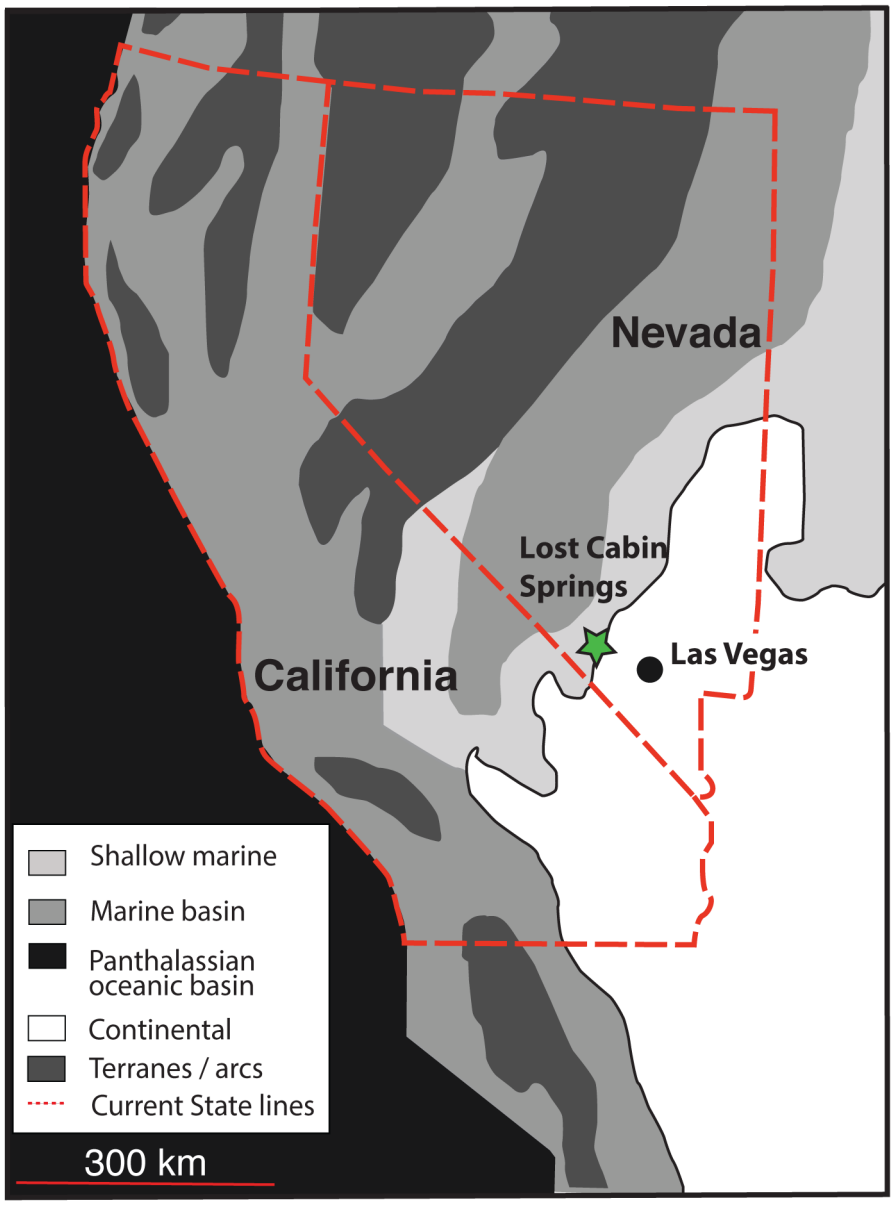

FIGURE 2: Early Triassic paleogeographic reconstruction of the western US. The Lost Cabin Springs Locality is denoted with a green star and the various shades depict the depositional environment during the Early Triassic (modified from Hoffmann *et al.*, 2013).

Specimens here included were deposited in the collections of the Natural History Museum (MnhnL OPH) and the Muschelkalkmuseum Ingelfingen (MHI).

The terminology used herein follows Stöhr *et al.* (2012) and Thuy & Stöhr (2011, 2016). We adopt the classification proposed by O'Hara *et al.* (2017, 2018). The extreme fragility of the skeletal plates, however, precluded detachment and re-mounting of the lateral arm plates. As a result, we were unable to illustrate the external and internal sides of the same lateral arm plates using scanning electron microscopy, as is a common practice in ophiuroid descriptions (Thuy & Numberger-Thuy 2021).

We scored the skeletal plates following Thuy & Stöhr (2016, 2018), referring to the same character definitions and acronyms and using the character matrix elaborated by Thuy & Stöhr (2016) and modified by Thuy & Stöhr

(2018) but excluding *Inexpectacantha acrobatica* Thuy, 2005 because of its ambiguous taxonomic affinities (Thuy & Numberger-Thuy 2021). The character matrix including the scores of the ophiuroid material described in the present paper is shown in Table 1. Bayesian inference analysis was performed using MrBayes (Huelsenbeck & Ronquist 2001) which relies on a modified version of the Juke-Cantor model for morphological data as outlined by Lewis (2001), with variable character states from 2 to 10 (Wright & Hillis 2014). Only variable characters were sampled, and we compensated for character selection bias by letting MrBayes search for parsimony informative characters (Mkpars model) (Wright & Hillis 2014). All character states were assumed to have equal frequency, and prior probabilities were equal for all trees. We assumed that evolutionary rates vary between sites according to a discrete gamma distribution. Average standard deviations of split frequencies stabilized at about 0.008 after 3 million generations (mgen), sampled every 1,000 generations. The first 25% of the trees were discarded as burnin. The consensus trees were examined with the software FigTree v. 1.4.2 by Rambaut (http://tree.bio.ed.ac.uk/software/figtree/). Confidence intervals of 95–99% were regarded as strong support for a node to be true, and at least 90% probability as good support.

Results

Preservation of the ophiuroid remains

The ophiuroid fragments described herein were found in insoluble residues of one packstone sample (LC–18–34). The insoluble residues from this sample were dominated by ophiuroid fragments with very few other fossils preserved. The most abundant fragments in this sample were vertebrae, which were brown to amber in color. These were all likely preserved as stereomic molds, with minerals infilling and replacing parts of the skeletal elements, so the stereomic structure is well preserved and visible in SEM imagery.

Phylogenetic analysis

The Bayesian estimate resulted in a well-resolved tree (Fig. 3) with good support for most of the clades. The ophiuroid taxon described herein (*Ophiosuperstes praeparvus* gen. et sp. nov.) holds a basal position in the tree, sister to the Ophintegrida clade. This node gains high posterior probability (96 %), suggesting a robust phylogenetic relationship. The Ophintegrida clade is almost fully resolved, including a basal split into an Ophiacanthida-Ophioscolecida clade (but including the Ophioleucida) and an Amphilepidida clade. The other Triassic ophiuroid included in the tree, *Aplocoma agassizi*, holds a more derived position than *Ophiosuperstes praeparvus*, being situated at the base of the Ophiodermatina.

Systematic palaeontology

Class Ophiuroidea Gray, 1840

Subclass Myophiurida Matsumoto, 1915

Infraclass Metophiurida Matsumto, 1913

Superorder Ophintegrida O'Hara, Hugall, Thuy, Stöhr & Martynov, 2017

Order unknown

Family unknown

Genus *Ophiosuperstes* nov.

TABLE 1 : Character matrix

	1 – 10	11 – 20	21 – 30	31 – 40	41 – 50	51 – 60	61 – 70	71 – 80	81 – 90	91 – 100	101 – 110	111 – 120	121 – 130
Aganaster gregarius	010000?0--	0000100211	??00--?010	132100??1?	?-?000??11	0000000110	0000000000	?0000-1000	00?0011110	1110020100	0003211010	10-------1	0100010--0
Amphilepis norvegica	11000000--	0020002211	3100--0021	1320002120	1-10002011	0000010110	0000200012	00010-101-	---1011110	1010010000	01110001--	--11111000	1001---0-0
Amphilimna olivacea	11000?0300	0011002110	3100--0011	1401000101	0-10202011	0200100110	0101200012	00110-0002	0122011210	1120010000	02120011--	--11111000	0001---0-1
Amphioplus congensis	11011-00--	0013??021?	???0--0101	0321000110	0-20203100	130011010-	0001000012	10010-1001	10120?1210	1010010000	02120011--	--01111000	1001---113
Amphiura chiajei	11000000--	0010212212	1100--0011	1121001110	0-20203100	130011000-	0001000012	10010-1000	0012011210	1010010000	02110011--	--01111000	1001---113
Aplocoma agassizi	11001-?100	0010101011	2000--?000	132100??1?	0-00000011	0000000110	0001000001	00000-0000	1000001010	1110023000	00112001--	--20000110	1000010--1
Aspiduriella scutellata	000001?100	002310000?	??00--?010	1001100??0	011?????11	000000010-	0000000000	?0100-3004	0010001010	1000000100	0213011001	11-------0	1100001--0
Aspiduriella streichani	000001?100	002210000?	5000--0001	1001110??1	111??2????	??0010010-	0001000000	?0100-3004	0?10001010	1000000000	0013011001	11-------0	10?0001--?
Asteronyx loveni	3--11-20--	0020100200	5010--0011	1300000?03	1-00020001	02001?????	002----110	0110222003	0000000-00	0000000000	0213110000	??-------0	1??0300--1
Eirenura papillata	1101??2211	011210201?	0000--0100	1411100?11	0110001011	0000110110	1000100000	01100-0001	0111011010	1121120102	01112001--	--20001200	1000011--1
Euryale aspera	3--11-2100	0120100201	50?0--0011	1300010?1	0-11000001	021110100-	002----110	?100210103	0000100-00	0000000000	0203311001	??-------0	1000300--1
Gorgonocephalus caputmedusae	3--11-2300	0120100l0?	50?0--0021	1110110?03	1001020001	02111?????	0011200110	0110220003	0000100-00	1000000000	0203110002	00-------0	1000300--1
Hemieuryale pustulata	20100000--	002010020?	???0--0121	1101000121	0-10202011	0100100110	1011?00101	?0000-0000	1000000-00	1020013101	02113001--	--11110000	1000100--0
Histampica duplicata	10000000--	0010202211	3100--0011	1401000011	0-10002011	0100100110	0000000012	10010-2000	1001011010	1020010011	02120011--	--00101000	1001---101
Melusinaster alissawhitegluzae	??????????	??????????	??????????	??????????	??????????	???0??????	??????????	???????0??	???0000-10	1000000000	0013011001	00-------0	1010001--0
Ophiacantha bidentata	11011-0310	0110101010	3000--0020	1201000023	0-10002011	0000000110	1000000013	11010-2000	1101001011	0032023000	10100001--	--20000120	1000112--2
Ophiactis savignyi	11011-0300	0022200212	3100--0011	1121000212	0-20002100	0300100010	1000210012	?100101000	0101001010	1020010011	02120001--	--00101000	1001---103
Ophiarachna incrassata	11011-0110	0100121010	2000--1020	1021100121	0111010011	0000100110	1101111013	02010-0001	1?00001010	1120022100	32112001--	--20000110	1000210--1

.....continued on the next page

TABLE 1 : (continued)

	1 – 10	11 – 20	21 – 30	31 – 40	41 – 50	51 – 60	61 – 70	71 – 80	81 – 90	91 – 100	101 – 110	111 – 120	121 – 130
Ophienigma spinilimbatum	1000000310	0000202211	3110--0020	0201000113	0-20202011	0100110110	1001010012	00010-2001	1101001010	1020010010	02120001--	--00101000	1011---101
Ophiochiton fastigatus	10010000--	0010002212	3100--0021	1421100023	0120002011	0100100110	0001200012	?0010-2000	1012011110	1110010102	02120001--	--11110000	1000113--3
Ophiochondrus stelliger	11011-0110	0120101012	3000--0121	1201000210	0-10002011	0000010110	1000000011	?101101002	1101001011	0031023001	10100001--	--20100120	1000102--1
Ophiocopa spatula	11001-0100	0003101211	3000--0110	1321000221	0-10002011	0000000110	1000010013	11100-2000	1101001011	1032023000	10100001--	--20000120	1010112--2
Ophiocoma echinata	11011-0110	0100121011	2000--1010	1001000221	1-20013100	0400100110	1001111013	02010-2000	1000001010	1020020100	22100001--	--20000120	1010213--3
Ophiocomina nigra	11011-0110	0100101211	3100--0021	1201100223	1020110011	0000110110	0001000013	01010-2001	1101001011	1012020000	10100001--	--20000120	1010113--2
Ophiocten sericeum	10000000--	0000100211	5012110100	1400100010	0110020111	000000010-	0001100012	00010-2101	0001001210	0012020100	3103110003	00-------0	2000310--1
Ophioderma longicauda	11011-0110	0100121012	1000--1020	1021000113	0-21010011	0000100110	1101111000	02100-0000	1000011010	1120022101	32112001--	--20000110	1000210--1
Ophiodoris malignus	11001-00--	0000002211	3101000010	0021000121	0-20002011	0100100110	0001200012	00010-1000	1112011110	1020010101	02120001--	--10110000	1010113--3
Ophiolepis superba	20001-00--	0010110212	3110--0000	1301000121	0-20202011	0100100110	0011100000	0?010-0000	1000011010	1010022101	32120011--	--11110000	1000200--0
Ophioleuce seminudum	1001000110	0100002011	3101000000	1321000110	0-00101011	0000000110	100112?001	01010-3000	1101011010	1121123002	01113001--	--20001200	1010111--0
Ophiolimna bairdi	11011-0210	0100101011	3000--0110	1201000023	0-10102011	0000000110	1000020012	11010-2001	1101001011	1012020001	10100001--	--20001120	1000112--2
Ophiolycus purpureus	11011-1100	0100101012	3000--0021	1221000003	1-10110011	0000110110	0?1110?012	0100111002	0101011011	1100000101	00100001--	--20000110	1010111--1
Ophiomusium lymani	20000000--	0020100202	5012020100	1311000020	0-10200011	0000000110	0000000000	00000-0000	1000011110	0010021100	0013211013	11-------1	0100010--0
Ophiomyces delata	01011-0300	1------112	0000--0000	0321110112	0110101011	0100010111	1000000012	01110-1000	0111001010	1112020100	01112001--	--20001200	1000111--2
Ophiomyxa pentagona	3--11-20--	0000121211	2000--1010	1001000010	0-21000011	0000110110	0001100000	010010101-	---0001010	1100003100	00112011--	--20000110	1000210--1
Ophionereis porrecta	10011-00--	0000002212	3101000010	0021000121	0-20003110	0300100110	1011210012	00010-1000	1013001110	1020010100	02120001--	--10110000	1010113--3
Ophiopallas paradoxa	10011-0110	0100102012	3101010100	0321000021	0-00200011	0000100110	1001121001	0101111000	1?01011010	1121121002	01120001--	--20001200	1010111--0

.....continued on the next page

TABLE 1 : (continued)

	1 – 10	11 – 20	21 – 30	31 – 40	41 – 50	51 – 60	61 – 70	71 – 80	81 – 90	91 – 100	101 – 110	111 – 120	121 – 130
Ophiopholis aculeata	10101-0211	0110202110	4100--0021	1101000222	1-20113100	1300111010	1011210012	0101111000	0103011010	1020010010	22120011--	--20100100	1001---213
Ophioplax lamellosa	10001-00--	0000202012	3101000110	1321000121	0-10002011	0100100110	0001200012	00000-1000	1012011210	1010010101	02120001--	--10110000	1010113--3
Ophiopsila guineensis	11011-00--	0010302211	3100--0011	1021000112	1-20203100	0300110110	0001200012	00100-0004	1102011110	1100010000	02110011--	--11111000	0011---0-1
Ophioscolex glacialis	3--11-20--	1------210	3000--0020	1200000203	1-00111011	0000100110	002----012	01010-201-	---0011011	1100020102	02100001--	--20100000	0010111--0
Ophiotholia spatifer	110???00--	1------212	0000--0000	0321110112	0110101011	0100000111	0000000012	01010-1000	0111001011	1112020101	01112001--	--20101000	0000111--1
Ophiothrix fragilis	1110010301	0020002110	4100--0020	010102----	2-10113100	1300111110	1001110013	0101211002	0003011010	1020010010	22120011--	--20100100	1001---203
Ophiotreta valenciennesi	11011-0110	0110101010	3100--1010	1321000111	1-10110011	0000100110	0001000013	?1110-2000	1101011011	1012020000	10100001--	--20000120	1000113--2
Ophiozonella longispina	10000000--	0010100212	3110--0010	1301000120	0-20002111	0200100110	1001111012	00010-2000	1000011010	1120023101	32133011--	--11110000	1000200--0
Ophiura ophiura	10000000--	0010100211	5112120100	1400100113	1110020011	000000010-	0001100001	00100-2100	0011011210	0011020100	3200111013	00-------0	2000300--1
Palaeocoma milleri	100????110	0020100010	5012120100	1311000110	0-1001??11	0000110110	0001100000	00100-2000	0010001010	1010021101	3213111013	00-------0	1100010--1
Sigsbeia murrhina	20100000--	00201?020?	???0--?020	1101002010	0-1???????	??00101110	1011010100	00100-3100	1?00010-10	1020012101	02033001--	--11110000	1000100--0
Praeparvus superstesii	??????????	0???100???	??????????	??????????	????????11	00?0?00110	00?????00?	???????0??	???0011010	1010020102	02130001--	--20000200	1100000--0

Etymology. *Ophiosuperstes* n. gen. is derived from the Latin adjective *superstes* meaning survivor, referring to the occurrence in the aftermath of the end-Permian mass extinction. Gender masculine.

Type and only species. *Ophiosuperstes praeparvus* sp. nov.

Diagnosis. as for the species, by monotypy.

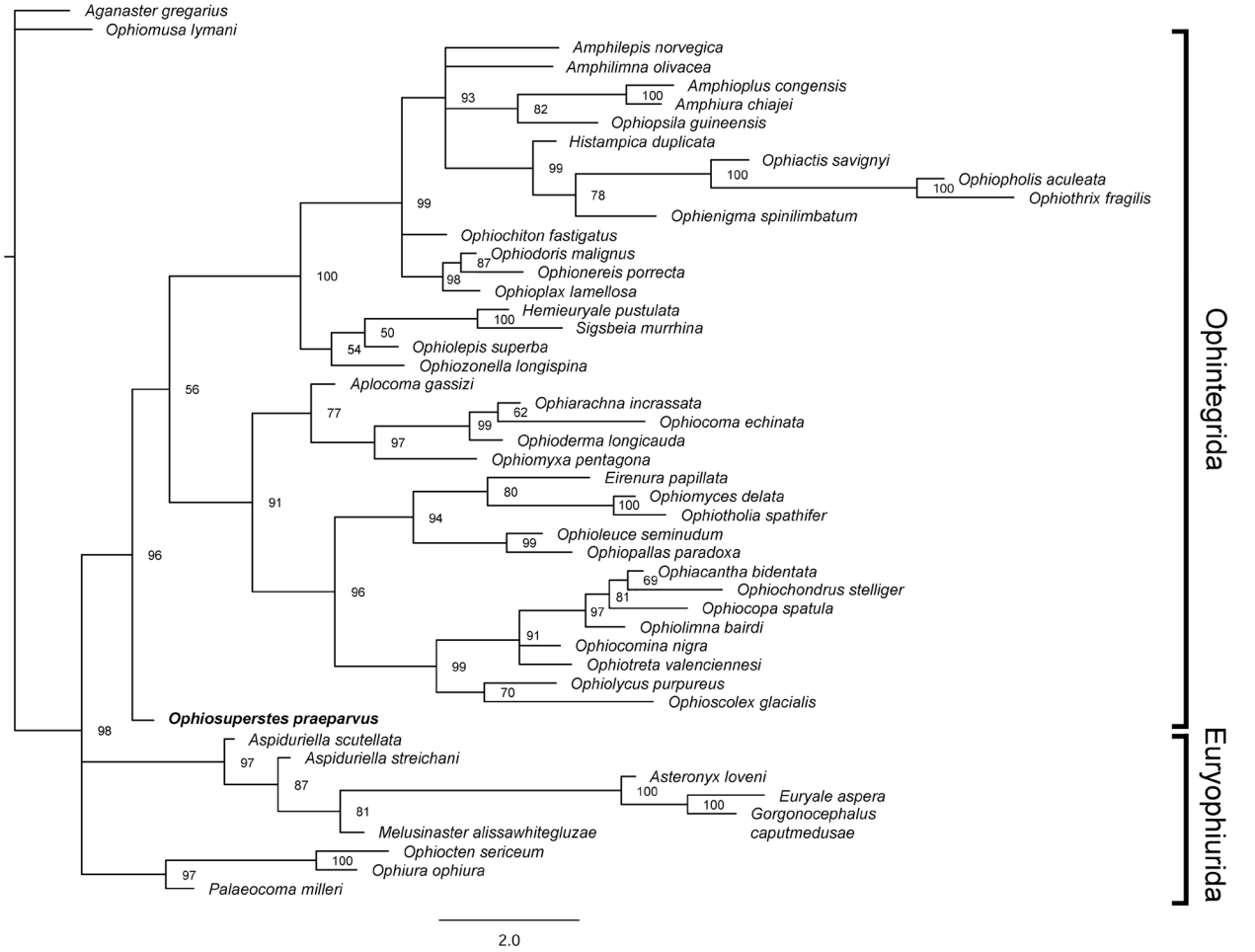

FIGURE 3: Morphology-based phylogenetic tree inferred using MrBayes, showing the position of *Ophiosuperstes praeparvus* gen. et sp. nov. (marked in bold). Numbers at nodes indicate posterior probabilities.

Ophiosuperstes praeparvus **gen. et sp. nov.**

Figs. 4–5

Etymology. *praeparvus* is Latin for very small or minute, as these microfossils were extracted from a small shelly fossil-style assemblage.

Holotype. MnhnL OPH177

Paratypes. MnhnL OPH178 – 190

Type locality. Lost Cabin Springs locality, southern Nevada (Maxwell *et al.* 2020).

Type stratum. Bed LC–18–34 within the Virgin Limestone Member of the Moenkopi Formation, Spathian, lower Triassic.

Diagnosis. Ophintegrid ophiuroid with stout lateral arm plates of rounded outline, very weak oblique elongated spur on ventro-proximal tip of outer surface, otherwise devoid of spurs or conspicuous outer surface ornamentation; with up to six small, vertical spine articulations slightly sunken into distal edge of lateral arm plate, composed of arched, shifted dorsal and ventral lobes merged at their proximal tips and encompassing the muscle and nerve openings; no sigmoidal fold; tentacle openings developed as small notches lined by a shallow groove in proximal to median lateral arm plates, and reduced to a within-plate perforation in distal lateral arm plates; ventral arm plates trapezoid; radial shields rounded isosceles triangular, without extensions or incisions.

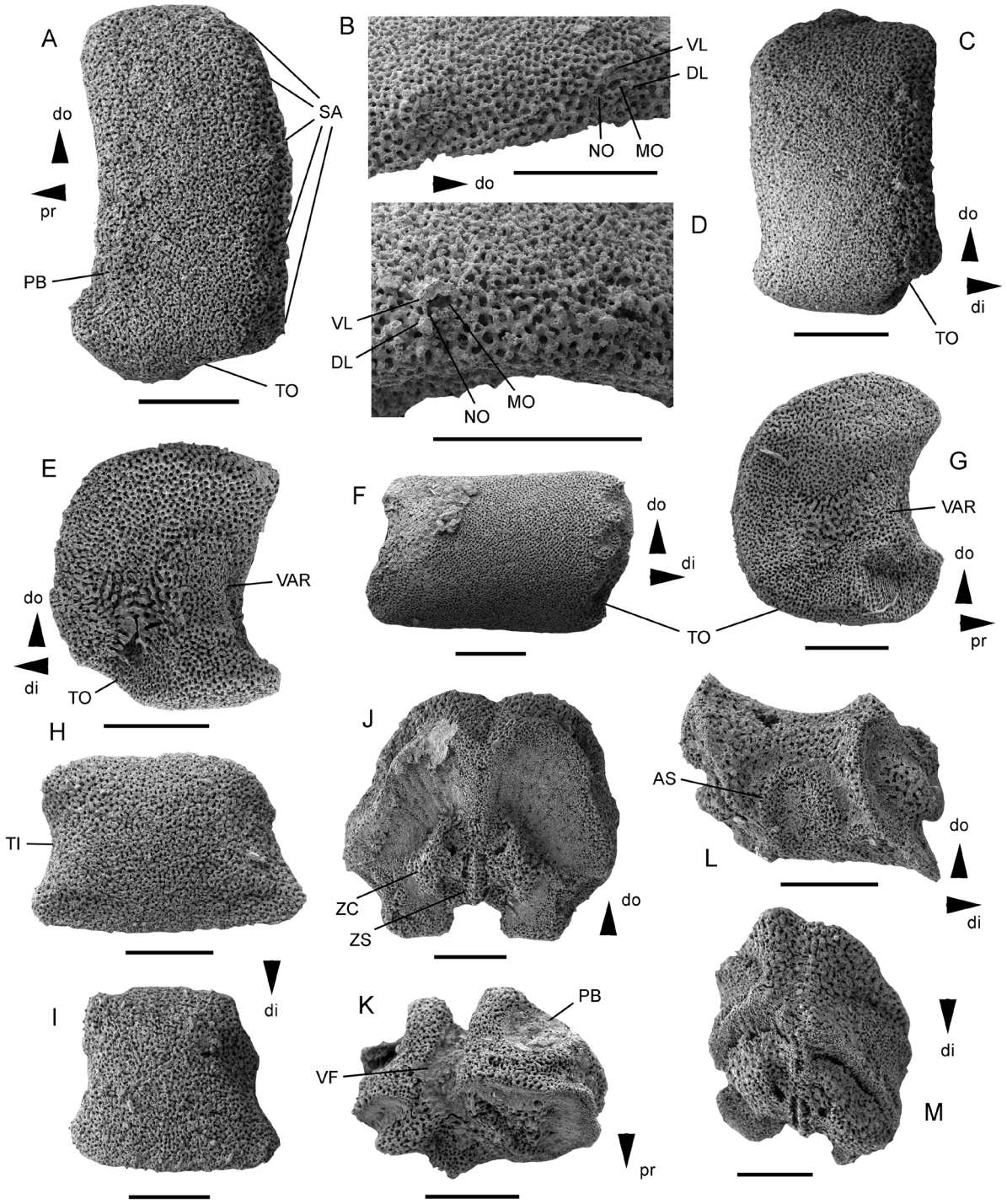

FIGURE 4: Dissociated arm plates of the ophiuroid *Ophiosuperstes praeparvus* gen. et sp. nov., from the Virgin Limestone Member of the Moenkopi Formation, Spathian, lower Triassic, Lost Cabin Springs locality, southern Nevada. A–B: holotype (OPH177), proximal lateral arm plate in external view (A) and with detail of spine articulations (B). C–D: paratype (OPH178), median lateral arm plate in external view (C) and with detail of spine articulations (D). E: paratype (OPH179), median lateral arm plate in internal view. F: paratype (OPH181), distal lateral arm plate in external view. G: paratype (OPH180), median lateral arm plate in internal view. H: paratype (OPH182), proximal ventral arm plate in external view. I: paratype (OPH183), median to distal ventral arm plate in external view. J: paratype (OPH184), proximal vertebra in distal view. K: paratype (OPH185), proximal vertebra in ventral view. L: paratype (OPH186), median vertebra in lateral view. M: paratype (OPH187), median vertebra in dorso-distal view. Abbreviations: AS: articular structure; di: distal; DL: dorsal lobe; do: dorsal; MO: muscle opening; NO: nerve opening; pr: proximal; PB: podial basin; SA: spine articulations; TO: tentacle opening; VAR: vertebral articular ridge; VF: ventral furrow; VL: ventral lobe; ZC: zygocondyle; ZS: zygosphene. All scale bars equal 0.2 mm.

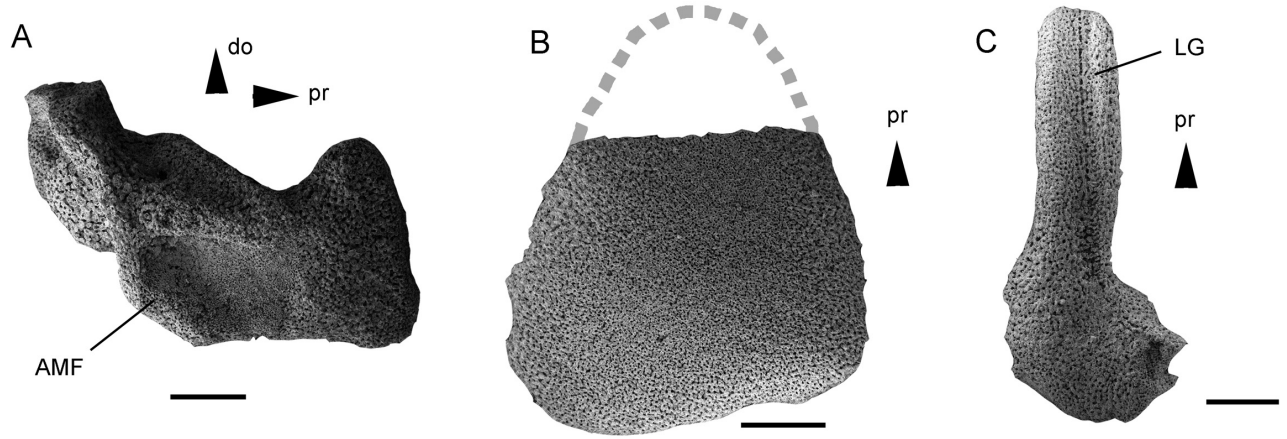

FIGURE 5: Dissociated disc plates of the ophiuroid *Ophiosuperstes praeparvus* gen. et sp. nov., from the Virgin Limestone Member of the Moenkopi Formation, Spathian, lower Triassic, Lost Cabin Springs locality, southern Nevada. A: paratype (OPH188), oral plate in abradial view. B: paratype (OPH189), radial shield in external view, with outline of missing proximal tip reconstructed using a dashed grey line. C: paratype (OPH190) adradial genital plate in dorsal view. Abbreviations: AMF: abradial muscle fossa; do: dorsal; LG: longitudinal groove; pr: proximal. All scale bars equal 0.2 mm.

Description of holotype. MnhnL OPH177 is a dissociated proximal lateral arm plate of stout, rounded outline, approximately two times higher than long, with rounded dorsal and distal edges and protruding ventro-proximal portion; outer proximal edge evenly concave, lined by a relatively broad but poorly defined band of slightly more coarsely meshed stereom with a faint horizontal striation but without spurs other than a very weak oblique elongated spur on the ventro-proximal tip of the outer surface (Fig. 4A); outer surface devoid of constriction, covered by a relatively finely meshed stereom with trabecular intersections transformed into very small tubercles; five relatively small, equal-sized spine articulations along the distal edge, with a slight dorsalward increase in the size of the gaps between the spine articulations, at the same level as the outer surface stereom; spine articulations (Fig. 4B) almost vertical, composed of arched and slightly shifted dorsal and ventral lobes encompassing a small muscle opening and a slightly smaller nerve opening; ventral edge with a small but well developed tentacle notch, lined by a shallow, poorly defined groove; inner side of lateral arm plate (not figured) with a large, well-defined, single vertebral articular ridge composed of the same stereom as the remaining inner side; inner distal edge without spurs; small but clearly defined tentacle notch; no perforations discernible.

*Paratype supplements and variation***.**

Lateral arm plates: median lateral arm plates (MnhnL OPH178 – OPH180) similar to holotype with respect to general outline, outer surface stereom (Fig. 4C), outer proximal edge, shape and position of spine articulations (Fig. 4D) and morphology of inner side (Fig. 4E, G) but with lower height/length ratio, fewer spine articulations (three to four) and smaller tentacle notch. Distal lateral arm plate (MnhnL OPH181) longer than high, of rounded rectangular outline with straight dorsal and ventral edges, with three closely-spaced spine articulations and with tentacle openings developed as within-plate perforation close to ventralmost spine articulation (Fig. 4F).

Vertebrae (MnhnL OPH184 – 187) roughly disc-shaped (proximal vertebrae, Fig. 4J, K) to cylindrical (median and distal vertebrae, Fig. 4L, M), with concave lateral saddle showing a single, tongue-shaped articular surface (Fig. 4L) with the lateral arm plate; large, straight dorsal muscle fossae and much smaller, straight ventral ones; distal face with dorsalwards converging zygocondyles and with a small zygosphene protruding only very little beyond the ventral edge of the zygocondyles (Fig. 4J); deep and broad ventral furrow with small podial basins (Fig. 4K).

Ventral arm plates (MnhnL OPH182 – 183) trapezoid, with weakly convex distal edge, concave lateral edges and narrower, rectangular proximal portion (Fig. 4H, I); no spurs or conspicuous outer surface ornamentation.

Oral plate (MnhnL OPH188) longer than high, slender, fragile, with abradial muscle fossa developed as central depression (Fig. 5A) and small adradial muscle attachment area lining ventral edge of adradio-distal articular surface.

Radial shield (MnhnL OPH189) with proximal portion broken, rounded isosceles triangular in extrapolated outline (Fig. 5B), no signs of extensions or incisions.

Adradial genital plate (MnhnL OPH190) bar-like, with a longitudinal groove and a swollen distal end (Fig. 5C).

Remarks. The ophiuroid remains described in the present paper include various types of skeletal components, i.e. lateral and ventral arm plates, vertebrae, oral plates, genital plates and fragmentary radial shields. The ossicles of every component type show very little variation other than the changes depending on the position within the arm (e.g. Thuy & Stöhr 2011). In particular, the lateral arm plates all belong to the same species, as indicated by the similarities in plate proportions, outer surface ornamentation, spine articulation morphology and position, and vertebral articular structure morphology (Thuy & Stöhr 2011). Furthermore, the various types of ossicles are of compatible size and, in some cases, show corresponding articulation surfaces, e.g. the vertebral articular ridge on the inner side of the lateral arm plates matching the lateral articular ridge of the vertebrae. We therefore conclude that all the ophiuroid remains belong to the same species.

The spine articulations of the lateral arm plates described in the present paper are composed of small muscle and nerve openings encompassed by a ventral and dorsal lobe. This configuration precludes assignment to the Euryophiurida, whose spine articulations lack dorsal and ventral lobes and have the muscle and nerve openings separated by a vertical ridge (O'Hara *et al*, 2018), and instead suggests assignment to the Ophintegrida. Within that superorder, affinities are not clear-cut because the lateral arm plates and the other skeletal parts lack characters that are uniquely found in one of the orders. This observation is in line with our phylogenetic estimate in which the ophiuroid described herein holds a basalmost position at the stem of the Ophintegrida.

Comparison with other fossil ophiuroids is hampered by the lack of detailed morphological analyses. Most descriptions of Triassic ophiuroids published to date are superficial and poorly illustrated, omitting important characters such as lateral arm plate microstructures that have been identified as systematically relevant (e.g. Thuy & Stöhr 2016; O'Hara *et al.* 2018). *Praeaplocoma hessi* Broglio Loriga & Berti Cavicchi, 1972 from the lower Triassic of Italy shares some superficial similarities with the ophiuroid described herein, in particular regarding the outline of the radial shields and the shape of the ventral arm plates. The lateral arm plates of *P. hessi*, however, are bulging. The most important difference, however, was revealed by scanning electron microscopy of newly collected specimens from the Dolomites, close to the type area of the species (Twitchett *et al.* 2005), showing that the spine articulations of *P. hessi* lack dorsal and ventral lobes and instead have their muscle and nerve openings separated by a vertical ridge (Fig. 6). This observation places *Praeaplocoma* in the superorder Euryophiurida and allows a clear distinction from the ophiuroid described herein.

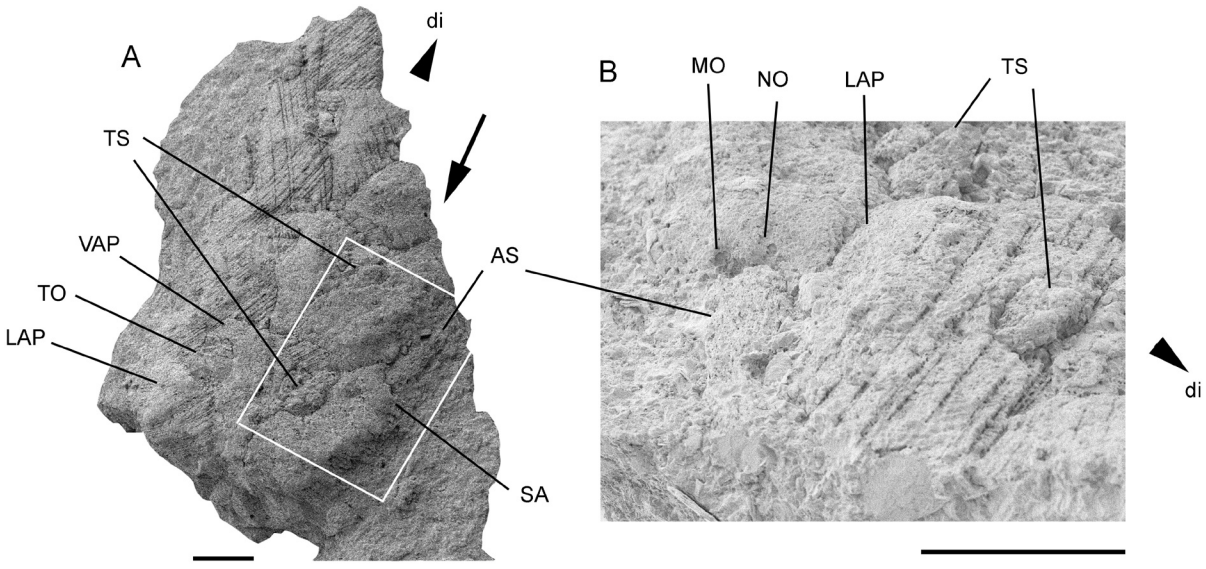

FIGURE 6: Arm fragment of *Praeaplocoma hessi* Broglio Loriga & Berti Cavicchi, 1972, (MHI 1307/nnn) from the Werfen Formation, Lower Triassic, of Weißhorn, Italy. A: arm fragments in ventral view. B: detail of part marked by white rectangle in A. Abbreviations: AS: arm spine; di: distal; LAP: lateral arm plate; MO: muscle opening; NO: nerve opening; SA: spine articulation; TO: tentacle opening; TS: tentacle scale; VAP: ventral arm plate. All scale bars equal 0.2 mm. Arrow in A indicates direction of view shown in B; refer to tentacle scales (TS) for better correspondence between A and B.

Shoshonura brayardi Thuy, 2019 from the lower Triassic of Idaho is another confirmed basal member of the Ophintegrida. It differs from the ophiuroid described herein in the more bulging lateral arm plates and the deeper tentacle notches of the ventral arm plates. Furthermore, the spine articulations are typical of the ophintegrid order Ophiacanthida. *Arenorbis squamosus* (Picard, 1858) from the middle Triassic of central Europe has lateral arm plates with several spurs along the outer proximal edge, and a slightly raised distal portion with larger, unambiguously ophiodermatid-like spine articulations.

Closest similarities are shared with the middle to upper Triassic genus *Aplocoma* d'Orbigny, 1852, in particular with respect to the shape of the lateral arm plates. In contrast to the ophiuroid described herein, however, *Aplocoma* has parallel rather than dorsalward converging zygocondyles on the distal vertebral articulations, ventral arm plates with a pointed rather than straight proximal edge, lateral arm plates with a ventralwards protruding ventro-distal tip and an outer proximal edge with spurs but lacking a fine horizontal striation, and spine articulations that are oblique rather than vertical and that have a weakly developed sigmoidal fold. These characters not only differentiate *Aplocoma* from the ophiuroid described herein but also suggest a more derived position of that genus within the Ophintegrida. Our phylogeny corroborates this assumption and places the type species of *Aplocoma*, *A. agassizi*, at the stem of the order Ophiodermatida, albeit with low support.

Because the ophiuroid described herein differs from all other unambiguously diagnosed fossil ophiuroids, we assign it to the new genus and species *Ophiosuperstes praeparvus*. For the time being, we prefer to eclipse the numerous poorly diagnosed lower Triassic ophiuroid taxa (e.g. Detre & Mihály 1987; Chen *et al.* 2004; Chen & McNamara 2006), because the morphological information available for these taxa is too superficial for a meaningful comparison. A detailed re-evaluation taking into account recent progress in ophiuroid systematics is necessary in order to determine whether the respective type specimens yield sufficient morphological information for an unambiguous diagnosis. Therefore, rather than extrapolating or perpetuating these questionable taxa, we prefer to introduce a new, unambiguously diagnosed taxon as a basis for future comparison.

Discussion

The results of the phylogenetic estimate suggest that *Ophiosuperstes praeparvus* gen. et sp. nov. holds a basalmost position within the Ophintegrida, which is one of the two superorders of the living Ophiuroidea (O'Hara *et al.* 2017, 2018). For a long time, the basal radiation of the modern ophiuroids was supposed to have taken place in the Early Triassic, following an extreme bottleneck at the end-Permian mass extinction (e.g. Smith *et al.* 1995). Molecular and palaeontological data published in recent years, however, show that the diversification of the modern ophiuroids was well under way long before the end-Permian mass extinction (e.g. O'Hara *et al.* 2014, 2017; Thuy *et al.* 2015, 2019). The existence of coeval but more derived ophiuroids such as *Shoshonura brayardi* Thuy, 2019 suggests that *Ophiosuperstes praeparvus* gen. et sp. nov. is probably a persisting member of a more ancient stem ophintegrid group.

The discovery of *Ophiosuperstes praeparvus* gen. et sp. nov. was only possible thanks to the highly unusual preservation of its fossils. In fact, elemental composition analysis using EDS confirmed that the skeletal elements are composed of calcium phosphate, implying that the original high-Mg calcite of the ophiuroid skeleton was completely replaced by apatite. Thanks to phosphatization, the ophiuroid ossicles were left unscathed by the dissolution of the hard, fossiliferous limestone. There has been some debate surrounding the mechanisms behind phosphatization during this time period, in particular phosphogenesis driven by high-energy mixing events (Freeman *et al.* 2013; Milam *et al.* 2017) versus phosphatization occurring in beds with low sedimentation rates and/or sedimentary hiatuses (Freeman *et al.* 2019,). Maxwell *et al.* (2020) observed a link between small shell size and phosphatization, and suggest phosphatization resulted from the combination of warm pore water with low levels of oxygen and the small particle size of the ophiuroid fragments.

Generally, the original high-Mg calcite of echinoderm ossicles recrystallizes into low-Mg calcite during diagenesis, filling the stereom pores and transforming the original porous ossicle into a massive calcite crystal (Gorzelak *et al.* 2016). The fact that stereom pores are preserved to the finest detail even inside the skeletal plates suggests either that phosphatization took place before calcite recrystallisation, or that recrystallisation exceptionally led to a perfect textural stereom preservation. This is in line with previous reports of phosphatized echinoderms, where excellent stereom preservation prevailed (Pisera 1994; Svensson 1999). To our knowledge, this is the first case of an unambiguous phosphatized ophiuroid.

Acknowledgments

We thank E. Smith, O. Leadbetter, T. McGann, R. Revolorio Keith, M. Slaymaker and A. Hagen for help in field collection, and we acknowledge C. Stark for both field assistance and initial analysis of the samples. We thank Smith Geosciences for generous funding for this project, and C. Sumrall for linking team members in this project. We thank Hans Hagdorn (Ingelfingen, Germany) who provided specimens of *Praeaplocoma hessi* for comparison. Finally, we thank Sabine Stöhr, Fred Hotchkiss and an anonymous reviewer whose comments greatly improved an earlier version of this manuscript.

Author contributions

VM and SBP collected the material and processed the samples; BT and VM picked the skeletal remains and produced the scanning electron microscope images; BT performed the phylogenetic analysis; VM and SBP performed the elemental composition analysis; VM and BT compiled the figures; BT took the lead in writing the manuscript; all authors contributed to the manuscript.

References

Botting, J.P., Brayard, A. & The Paris Biota Team (2019) A late-surviving Triassic protomonaxonid sponge from the Paris Biota, Idaho, USA. *Geobios*, 54, 5−11. https://doi.org/10.1016/j.geobios.2019.04.006

Brayard, A., Jenks, J.F., Bylund, K.G. & The Paris Biota Team. (2019) Earliest Spathian ammonoids and nautiloids from the Paris Biota and Bear Lake area: significance for regional-to-global stratigraphy and correlation. *Geobios*, 54, 13−36. https://doi.org/10.1016/j.geobios.2019.04.007

Brayard, A., Krumenacker, L.J., Botting, J.P., Jenks, J.F., Bylund, K.G., Fara, E., Vennin, E., Olivier, N., Goudemand, N., Saucède, T., Charbonnier, S., Romano, C., Doguzhaeva, L., Thuy, B., Hautmann, M., Stephen, D.S., Thomazo, C. & Escarguel, G. (2017) Unexpected Early Triassic marine ecosystem and the rise of the Modern evolutionary fauna. *Science Advances*, 3, e1602159. https://doi.org/10.1126/sciadv.1602159

Broglio Loriga, C. & Berti Cavicchi, A. (1972) *Praeaplocoma hessi* n. gen., n. sp., un Ofiura del Werfeniano (Trias Inferiore) del Gruppo della Costabella, Dolomiti. *Memorie Geopaleontologiche dell' Universita di Ferrara*, 2 (1), 185−197.

Charbonnier, S., Brayard, A. & The Paris Biota Team (2019) New thylacocephalans from the Early Triassic Paris Biota (Idaho, U.S.A.). *Geobios*, 54, 37−43. https://doi.org/10.1016/j.geobios.2019.04.005

Chen, Z.Q. & Mcnamara, K.J. (2006) End-Permian extinction and subsequent recovery of the Ophiuroidea (Echinodermata). *Palaeogeography, Palaeoclimatology, Palaeoecology*, 236, 321−344. https://doi.org/10.1016/j.palaeo.2005.11.014

Chen, Z.Q., Shi, G.R. & Kaiho, K. (2004) New ophiuroids from the Permian/Triassic boundary beds of South China. *Palaeontology*, 47, 1301−1312. https://doi.org/10.1111/j.0031-0239.2004.00406.x

Detre, C. & Mihály, S. (1987) Két Újabb Ophiuroida Lelet A Balaton-Felvidék Triászából. *A Magyar Állami Földtani Intézet Évi Jelentése Az*, 1985, 449−452.

Doguzhaeva, L.A., Brayard, A., Goudemand, N., Krumenacker, L.J., Jenks, J.F., Bylund, K.G., Fara, E., Olivier, N., Vennin, E. & Escarguel, G. (2018) An Early Triassic gladius associated with soft tissue remains from Idaho, USA-a squid-like coleoid cephalopod at the onset of Mesozoic Era. *Acta Palaeontologica Polonica*, 63, 341−355. https://doi.org/10.4202/app.00393.2017

d'Orbigny, A.D. (1852) s.n. *In*: *Cours élémentaire de paléontologie et de géologie stratigraphiques. 2 (2).* Masson, Paris, pp. 381−849.

Erwin, D.H. (1993) *The Great Paleozoic Crisis: life and death in the Permian*. Columbia University Press, New York, New York, 327 pp.

Freeman, R.L., Dattilo, B.F. & Brett, C.E. (2019) An integrated stratinomic model for the genesis and concentration of ‚small shelly fossil' ‐ style phosphatic microsteinkerns in not ‐ so ‐ exceptional conditions. *Palaeogeography, Palaeoclimatology, Palaeoecology*, 535, 109344. https://doi.org/10.1016/j.palaeo.2019.109344

Freeman, R.L., Dattilo, B.F., Morse, A., Blair, M., Felton, S. & Pojeta, J. (2013) The ‚Curse Of Rafinesquina:' negative taphonomic feedback exerted by strophomenid shells on storm ‐ buried Lingulids In The Cincinnatian Series (Katian,

Ordovician) of Ohio. *Palaois*, 28, 359−372.
https://doi.org/10.2110/palo.2012.p12-094r
Gorzelak, P., Krzykawski, T. & Stolarski, J. (2016) Diagenesis of echinoderm skeletons: Constraints on paleoseawater Mg/Ca reconstructions. *Global and Planetary Change*, 144, 142−157.
https://doi.org/10.1016/j.gloplacha.2016.07.010
Hagdorn, H. (2018) Slipped through the bottleneck: *Lazarechinus mirabeti* gen. et sp. nov., a Paleozoic-like echinoid from the Triassic Muschelkalk (late Anisian) of East France. *Paläontologische Zeitschrift*, 92, 267−282.
https://doi.org/10.1007/s12542-017-0393-1
Hoffmann, R., Hautmann, M., Wasmer, M. & Bucher, H. (2013) Palaeoecology of the Spathian Virgin Formation (Utah, USA) and Its Implications for the Early Triassic Recovery. *Acta Palaeontologica Polonica*, 58, 149−173.
Huelsenbeck, J.P. & Ronquist, F. (2001) MRBAYES: Bayesian inference of phylogenetic trees. *Bioinformatics*, 17, 754−755.
https://doi.org/10.1093/bioinformatics/17.8.754
Lewis, P.O. (2001) A likelihood approach to estimating phylogeny from discrete morphological character data. *Systematic Biology*, 50, 913−925.
https://doi.org/10.1080/106351501753462876
Marzolf, J.E. (1993) Palinspastic reconstruction of early Mesozoic sedimentary basins near the latitude of Las Vegas; implications for the early Mesozoic Cordilleran cratonal margin. *In*: Dunne, G.C. & McDougall, K. (Eds.), *Mesozoic Paleogeography of the Western United States*, II, SEPM, Book 71, pp 433−462.
Matsumoto, H. (1915) A new classification of the Ophiuroidea: with description of new genera and species. *Proceedings of the Academy of Natural Sciences of Philadelphia*, 68, 43−92.
Maxwell, V., Thuy, B. & Pruss, S.B. (2020) An Early Triassic small shelly fossil‐style assemblage from the Virgin Limestone Member, Moenkopi Formation, western United States. *Lethaia*, 54, 368−377.
https://doi.org/10.1111/let.12409
Milam, M.J., Meyer, D.L., Datillo, B.F. & Hunda, B.R. (2017) Taphonomy of an Ordovician crinoid lagerstätte from Kentucky. *Palaios*, 32, 166−180.
https://doi.org/10.2110/palo.2016.048
O'Hara, T.D., Hugall, A.F., Thuy, B. & Moussalli, A. (2014) Phylogenomic Resolution of the Class Ophiuroidea Unlocks a Global Microfossil Record. *Current Biology*, 24, 1874−1879.
https://doi.org/10.1016/j.cub.2014.06.060
O'Hara, T.D., Hugall, A.F., Thuy, B., Stöhr, S. & Martynov, A.V. (2017) Restructuring higher taxonomy using broad-scale phylogenomics: The living Ophiuroidea. *Molecular Phylogenetics and Evolution*, 107, 415−430.
https://doi.org/10.1016/j.ympev.2016.12.006
O'Hara, T.D., Stöhr, S., Hugall, A.F., Thuy, B. & Martynov, A. (2018) Morphological diagnoses of higher taxa in Ophiuroidea (Echinodermata) in support of a new classification. *European Journal of Taxonomy*, 416, 1−35.
https://doi.org/10.5852/ejt.2018.416
Picard, E. (1858) Über den Keuper bei Schlotheim in Thüringen und seine Versteinerungen. *Zeitschrift für die Gesamten Naturwissenschaften*, 11, 425−436.
Pisera, A. (1994) Echinoderms of the Mójcza Limestone. *In*: Dzik, J., Olempska, E. & Pisera, A. (Eds.) Ordovician carbonate platform ecosystem of the Holy Cross Mountains, Poland. *Palaeontologia Polonica, Warsaw*, 53, pp. 283−307.
Poborski, S.J. (1954) Virgin Formation (Triassic) of the St. George, Utah, area. *Geological Society of America Bulletin*, 65, 971−1006.
https://doi.org/10.1130/0016-7606(1954)65[971:VFTOTS]2.0.CO;2
Pruss, S.B., Fraiser, M.L. & Bottjer, D.J. (2004) Proliferation of Early Triassic wrinkle structures: implications for environmental stress following the end‐Permian mass extinction. *Geology*, 35, 461−465.
https://doi.org/10.1130/G20354.1
Pruss, S.B. & Bottjer, D.J. (2004) Late Early Triassic microbial reefs of the western United States: a description and model for their deposition in the aftermath of the end-Permian mass extinction, *Palaeogeography, Palaeoclimatology, Palaeoecology*, 211, 127−37.
https://doi.org/10.1016/j.palaeo.2004.05.002
Pruss, S.B., Corsetti, F.A. & Bottjer, D.J. (2005) The unusual sedimentary rock record of the Early Triassic: a case study from the southwestern United States. *Palaeogeography, Palaeoclimatology, Palaeoecology*, 222, 33−52.
https://doi.org/10.1016/j.palaeo.2005.03.007
Reif, D.M. & Slatt, R.M. (1979) Red bed members of the Lower Triassic Moenkopi Formation, southern Nevada; sedimentology and paleogeography of a muddy tidal flat deposit. *Journal of Sedimentary Petrology*, 49, 869−889.
https://doi.org/10.1306/212F7865-2B24-11D7-8648000102C1865D
Romano, C., Argyriou, T., Krumenacker, L.J. & The Paris Biota Team. (2019) Chondrichthyan teeth from the Early Triassic Paris Biota (Bear Lake County, Idaho, USA). *Geobios*, 54, 63−70.
https://doi.org/10.1016/j.geobios.2019.04.001
Saucède, T., Vennin, E., Fara, E., Olivier, N. & The Paris Biota Team. (2019) A new holocrinid (Articulata) from Idaho (USA) highlights the high diversity of Early Triassic crinoids. *Geobios*, 54, 45−53.
https://doi.org/10.1016/j.geobios.2019.04.003

Schubert, J.K. & Bottjer, D.J. (1995) Aftermath of the Permian‐Triassic mass extinction event: paleoecology of Lower Triassic carbonates in the Western USA. *Palaeogeography, Palaeoclimatology, Palaeoecology*, 116, 1−39. https://doi.org/10.1016/0031-0182(94)00093-N

Sepkoski, J.J. Jr. (1981) A factor analytic description of the Phanerozoic marine fossil record. *Paleobiology*, 7, 36−53. https://doi.org/10.1017/S0094837300003778

Smith, A.B., Paterson, G.L.J. & Lafay, B. (1995) Ophiuroid phylogeny and higher taxonomy: morphological, molecular and palaeontological perspectives. *Zoological Journal of the Linnean Society*, 114, 213−243. https://doi.org/10.1006/zjls.1995.0024

Stöhr, S., O'Hara, T.D. & Thuy, B. (2012) Global diversity of Ophiuroidea. *PLOS ONE*, 7 (3), e31940. https://doi.org/10.1371/journal.pone.0031940

Svensson, A.M. (1999) Phosphatized echinoderm remains from upper Lower Ordovician strata of northern Öland, Sweden : preservation, taxonomy and evolution. *Examensarbete I geologi vid Lunds Universitet, Historisk geologi och paleontologi*, 105, 1−60.

Thompson, J.R., Hu, S., Zhang, Q.Y., Petsios, E., Cotton, L.J., Huang, J.Y., Zhou, C., Wen, W. & Bottjer, D.J. (2018) A new stem group echinoid from the Triassic of China leads to a revised macroevolutionary history of echinoids during the end-Permian mass extinction. *Royal Society Open Science*, 5, 171548. https://doi.org/10.1098/rsos.171548

Thuy, B., Escarguel, G. & The Paris Biota Team. (2019) A new brittle star (Ophiuroidea: Ophiodermatina) from the Early Triassic Paris Biota (Bear Lake County, Idaho, USA). *Geobios*, 54, 55−61. https://doi.org/10.1016/j.geobios.2019.04.004

Thuy, B., Hagdorn, H. & Gale, A.S. (2017) Paleozoic echinoderm hangovers: Waking up in the Triassic. *Geology*, 45 (6), 531−534. https://doi.org/10.1130/G38909.1

Thuy, B., Kutscher, M. & Bartosz, P.J. (2015) A new brittle star from the early Carboniferous of Poland and its implications on Paleozoic modern-type ophiuroid systematics. *Acta Palaeontologica Polonica*, 60, 923−929. https://doi.org/10.4202/app.00093.2014

Thuy, B. & Numberger-Thuy, L.D. (2021) Brittlestar diversity at the dawn of the Jenkyns Event (early Toarcian Oceanic Anoxic Event): new microfossils from the Dudelange drill core, Luxembourg. *Geological Society, London, Special Publications*, 514, 83−119. https://doi.org/10.1144/SP514-2021-3

Thuy, B. & Stöhr, S. (2011) Lateral arm plate morphology in brittle stars (Echinodermata: Ophiuroidea): new perspectives for ophiuroid micropalaeontology and classification. *Zootaxa*, 3013, 1−47. https://doi.org/10.11646/zootaxa.3013.1.1

Thuy, B. & Stöhr, S. (2016) A new morphological phylogeny of the Ophiuroidea (Echinodermata) accords with molecular evidence and renders microfossils accessible for cladistics. *PLOS ONE*, 11 (5), e0156140. https://doi.org/10.1371/journal.pone.0156140

Thuy, B. & Stöhr, S. (2018) Unravelling the origin of the basket stars and their allies (Echinodermata, Ophiuroidea, Euryalida). *Scientific Reports*, 8, 8493. https://doi.org/10.1038/s41598-018-26877-5

Twitchett, R.J., Feinberg, J.M., O'Connor, D.D., Alvarez, W. & McCollum, L.B. (2005) Early Triassic Ophiuroids: their paleoecology, taphonomy and distribution. *Palaios*, 20, 213−223. https://doi.org/10.2110/palo.2004.p04-30

Twitchett, R.J. & Oji, T. (2005) Early Triassic recovery of echinoderms. *Comptes Rendus Paleovol*, 4, 531−542. https://doi.org/10.1016/j.crpv.2005.02.006

Wright, A.M. & Hillis, D.M. (2014) Bayesian Analysis Using a Simple Likelihood Model Outperforms Parsimony for Estimation of Phylogeny from Discrete Morphological Data. *PLoS ONE*, 9, e109210. https://doi.org/10.1371/journal.pone.0109210